上海交通大學

SHANGHAI JIAO TONG UNIVERSITY

# Project Report


Title： Multi-objective optimization of a parallel manipulator using genetic algorithms

Student: 周资崴

Student ID: 120020910093

School: School of Mechanical Engineering

Teacher: 张小群

上海交通大學
SHANGHAI JIAO TONG UNIVERSITY

# 目录

# 1. Background

The shoulder joint is one of the key components of the upper limb prosthesis of the human body. In view of the shortcomings of the shoulder joint of the current series configuration, a new parallel shoulder joint design and analysis method based on a spherical three-degree-of-freedom parallel mechanism is proposed.

A mathematical model of a three-degree-of-freedom spherical parallel mechanism was established, and 11 design parameters were determined. The expressions of the kinematics forward and inverse solutions were derived through the constraint relationship. The velocity Jacobian matrix and force Jacobian were derived based on the inverse kinematics matrix and analyze and solve the singular shape of the mechanism.

Starting from the three optimization goals of working space, dexterity and maximum torque, a set of mechanism parameters whose working space, dexterity and maximum torque meet the set conditions are determined by multi-objective optimization using genetic algorithm.

# 2. Motivation

Disabled people are special groups of people who need special care and attention. According to the survey results of the China Disabled Persons' Federation, the total number of persons with disabilities in China in 1987 was about 51.64 million. By the end of 2010, it will reach 85.02 million. By 2020, the total number of persons with disabilities will exceed 100 million, of which 30% are upper limb amputations. Patients; due to traffic accidents, occupational accidents and natural disasters, the number of patients with upper limb amputations is increasing at a rate of 200,000 to 250,000 per year [1]. Some upper-limb amputation patients have lost their basic social work ability, which prevents them from producing and living normally. Therefore, they urgently need upper-limb prostheses to compensate for physical defects and improve their self-care ability.

The structure and performance of the shoulder joint directly determine the overall performance of the upper limb prosthesis, such as maneuverability, load-bearing capacity and smoothness of movement. At present, most of the research and design of shoulder joints at home and abroad adopt the tandem

configuration, but in terms of the structure and principle of the human body, the movement of the human joints is driven by parallel muscle groups. Therefore, the shoulder joints of the tandem configuration are parallel. Not satisfying the objective reality of the human body, the shoulder joints in parallel configuration will be more in line with the requirements of bionics [4]. Therefore, according to the characteristics of human joints and the principle of bionic design, it is of great significance to introduce the parallel mechanism into the design of human joints. In addition, for the three degrees of freedom of the shoulder joint, three motors connected in series lead to a large shoulder joint size and mass, which is difficult to match the actual shoulder joint size of a person, increasing the weight of the entire shoulder joint [2]; The spherical parallel mechanism has 3 degrees of freedom, which is compatible with the characteristics of a shoulder joint with 3 degrees of freedom, and is conducive to compactness and lightness of the joint.

The three-degree-of-freedom spherical parallel mechanism is widely used in engineering practice. It not only has three rotational degrees of freedom similar to human shoulder joints, but also has the advantages of parallel mechanisms such as high stiffness, small motion inertia and no drift accumulation [3, 4]. The shoulder joint designed based on the 3-DOF spherical parallel mechanism has high rigidity, compact structure, high transmission accuracy, closer to the actual shoulder joint of the human body, and more suitable for the overall design of upper limb prosthesis, which has important innovative significance.

# 3. Pre-work

### 3. 1 The range of motion of the human shoulder joint

The movement of the shoulder joint, as shown in Figure 1, mainly includes the six movements shown in the figure. The range of motion of the shoulder joint under normal conditions is: outreach of 90°, adduction of 10°; flexion of 90°, extension of 20°; external rotation of 50°, and internal rotation of 40°.

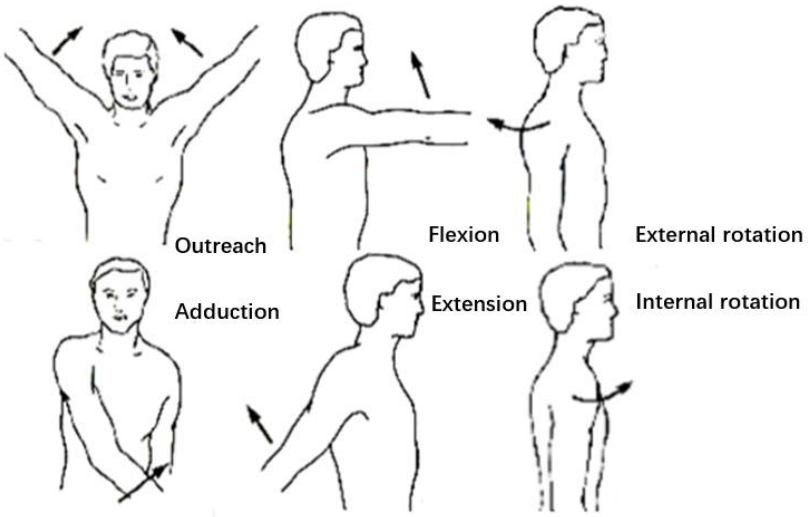


Figure1 Schematic diagram of the movement of the shoulder joint

Considering that the designed shoulder joint working space needs to meet the normal range of motion of the human body's actual shoulder joint, the designed range of motion is shown in Table 1.

Table 1 Designed range of motion

| movement | Ranges (° ) |
|---|---|
| Adduction-Outreach | [-10,90] |
| Flexion-Extension | [-90,20] |
| Internal rotation-External rotation | [-40,50] |

## 3.2 Modeling of spherical parallel mechanism

In the existing shoulder joint design, in order to realize the rotation of the shoulder joint with three degrees of freedom, the most common method is to use three motors in series to realize the rotation of three degrees of freedom. This kind of series combination of degrees of freedom can achieve greater work Space and simple control, but there are many shortcomings: the three motors and the reducer in series require a lot of space, which cannot meet the requirements of lightweight and miniaturization of the shoulder joint; the three drive motors are connected in series, and the motor located below is the upper motor Load, which will cause the shoulder joints designed in this way to drive very low efficiency and poor stiffness [5].

The three-degree-of-freedom spherical parallel mechanism (3-RRR) is composed of three branch chains. Each branch chain has three rotation pairs, and the axes of these three rotation pairs intersect the center of the sphere, as shown in Figure 2. Compared with the series configuration, this mechanism has many advantages: high efficiency, three-degree-of-freedom drive motors are installed on the static platform, and will not become the load of other motors; the moving platform is supported by three branch chains, so it has better The rigidity; the small moment of inertia can reduce the maximum torque of the drive motor to reduce the weight of the motor, which can meet the requirements of lightweight [6]. Although the three-degree-of-freedom spherical parallel mechanism also has the disadvantages of low dexterity and small working space, the actual range of motion of the human shoulder joint is not large enough, and the design standards of the shoulder joint can be considered in terms of working space and dexterity, so The shoulder joint of the parallel configuration can be used, and at the same time, good motion accuracy and working space can be achieved, and various performance indexes required by the shoulder joint can be met.

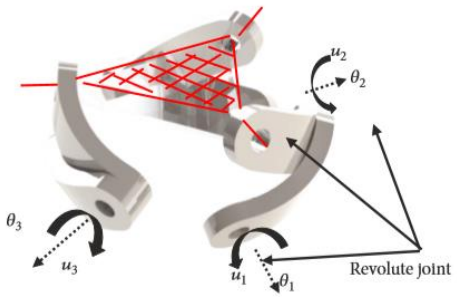


Figure2 Three-degree-of-freedom spherical parallel mechanism

### 3.3 Parameter definition

The shoulder of the prosthesis is modeled as a three-degree-of-freedom spherical parallel mechanism, as shown in Figure 2-4. The mechanism is composed of three branch chains, each branch chain has three rotation pairs, and the axes of these three rotation pairs all intersect at the center of the sphere, defined by the unit vectors $u_i$, $v_i$ and $w_i$ The characteristic angle of the connecting rod $\alpha_{1\_i}$ (connecting the static platform) is defined as α_(1_i), which represents the angle between the connected joints, and its approximate value range is: $0^\circ \leq \alpha_{1\_i} \leq 180^\circ$ . The characteristic angle of the connecting rod $b_i$ (connecting the moving platform) is defined as $\alpha_{2\_i}$, which represents the angle between the connected joints, and its approximate value range is: $0^\circ \leq \alpha_{2\_i} \leq 180^\circ$ .

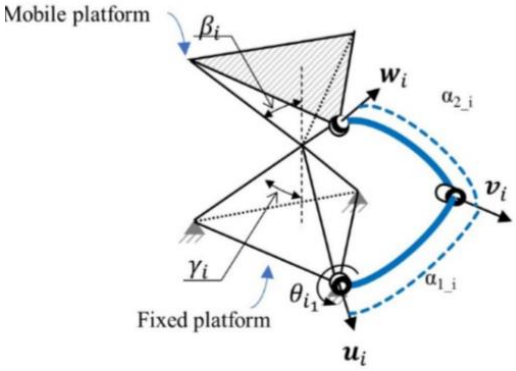


Figure 3 Schematic diagram of design parameters of spherical parallel mechanism

The moving platform and the static platform are usually triangular pyramids defined by an equilateral triangle and defined by $\beta_i$ and $\gamma_i$.

As shown in Figure 3, $\gamma_i$ is the half cone angle of the static platform. When $\gamma_i=0^\circ$ , the three driving motors are coaxial; when $\gamma_i=90^\circ$ , the three driving motors are on the same plane. When $\gamma_i<90^\circ$ , the center of the sphere is below the moving platform; when $\gamma_i> 90^\circ$ , the center of the sphere is above the moving platform. Therefore, in order to ensure sufficient assembly space, the approximate value range of $\gamma_i$ is: $0' \leqslant \gamma_i \leqslant 90^\circ$ so that the center of the sphere is below the moving platform. $\beta_i$ is the half cone angle of the moving platform. When $\beta_i=0°$, the three output shafts are coaxial. At this time, they degenerate into two degrees of freedom, so $\beta_i$ cannot be equal to 0°; when $\beta_i=90°$, the three output shafts are located at same plane. When $\beta_i<90°$, the center of the sphere is above the static platform, when $\beta_i>90°$, the center

of the sphere is above the static platform. Similarly, in order to ensure sufficient assembly space, the approximate value range of β_i is taken as: $0' < \beta_i \leqslant 90^\circ$ so that the center of the sphere is above the static platform.

It can be verified that when $\gamma_i$ and $\beta_i$ are larger, it is equivalent to the triangular pyramid being squashed, which reduces the link length of the branch chain, which is beneficial to avoid the interference between the branch chain links and the overall size of the shoulder joint, so $\gamma_i$ and $\beta_i$ should be as large as possible.

If the bottoms of the moving and static platforms are equilateral triangles, then the vertices of the bottoms are separated by 120°; but considering that the shape of the bottoms can be irregular triangles, the vertices of the bottoms in the static and moving platforms are considered as the parameter can take any value instead of a regular equilateral triangle. This means that the bottom surface is an oblique triangle, and each vertex of the bottom surface is defined by the angle $\delta_i$ (i represents the i-th branch, i = 1, 2, 3), which is regarded as another parameter of the mechanism. As shown in Figure 4, the angle $\delta_i$ is the angle between the y-axis and the axis of each vertex of the bottom surface.

In summary, the three-degree-of-freedom spherical parallel mechanism to be designed has 11 different structural parameters

$$\gamma, \beta, \alpha_{1\_1}, \alpha_{1\_2}, \alpha_{1\_3}, \alpha_{2\_1}, \alpha_{2\_2}, \alpha_{2\_3}, \delta_1, \delta_2, \delta_3.$$

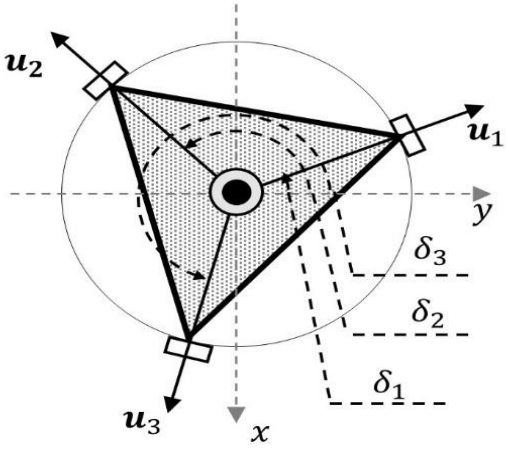


Figure 4 Distribution of vertices of the bottom triangle

### 3.4 Kinematic model

The inverse kinematics solution refers to the process of solving the angles $\theta_i(\mathrm{i}=1,2,3)$ of the three input $\alpha,\beta,\gamma$, and the analysis is as follows:

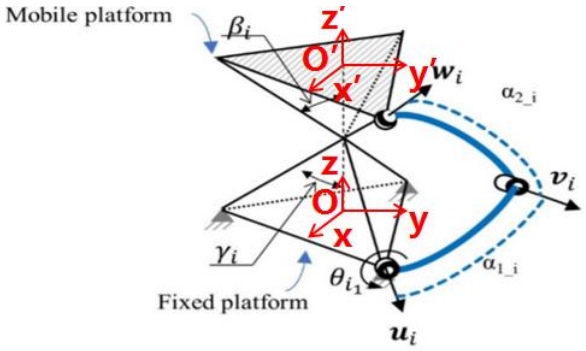


Figure 5 Coordinate system and direction vector diagram

As shown in Figure 5, the direction vector $u_i$ in the stationary platform fixed coordinate system O is expressed as

$$\mathrm{u_i} = \mathrm{R_z}(\delta_\mathrm{i})\mathrm{R_x}(\gamma - \pi/2)[0 \quad 1 \quad 0]^\mathrm{T}, \mathrm{i} = 1,2,3 \tag{3-1}$$

Among them, $R_a(b)$ represents a rotation of b degrees around the a axis.

the direction vector $v_i$ in the stationary platform fixed coordinate system O is expressed as

$$\mathrm{v_i} = \mathrm{R_z}(\delta_\mathrm{i})\mathrm{R_x}\left(\gamma - \frac{\pi}{2}\right)\mathrm{R_y}(\theta_\mathrm{i})\mathrm{R_z}(\alpha_{1_\mathrm{i}})[0 \quad 1 \quad 0]^\mathrm{T}, \mathrm{i} = 1,2,3 \tag{3-2}$$

the direction vector $w_i$ in the moving platform fixed coordinate system O is expressed as

$$\omega_i' = R_z(\delta_i)R_x\left(\frac{\pi}{2} - \beta\right)[0 \quad 1 \quad 0]^T, \mathrm{i} = 1,2,3 \tag{3-3}$$

Q is the azimuth matrix of the moving platform relative to the static platform, determined by the attitude change angle $\alpha,\beta,\gamma$

$$Q = R_Z(\gamma)R_y(\beta)R_x(\alpha) \tag{3-4}$$

The expression of $w_i$ in the stationary platform coordinate system O can be obtained by the transformation matrix Q and $\omega_i'$

$$w_i = Qw_i' = QR_z(\delta_i)R_x\left(\frac{\pi}{2} - \beta\right)[0 \quad 1 \quad 0]^T, \mathrm{i} = 1,2,3 \tag{3-5}$$

The driven rod needs to meet the following constraints

$$v_i \cdot w_i = \cos(\alpha_{2_i}) \tag{3-6}$$

Put the expressions of $v_i$ and $w_i$ into the formula, simplify the algebraic equation to obtain the relationship between the input angle $\theta_i(\mathrm{i} = 1,2,3)$ and the output attitude change angle $\alpha, \beta, \gamma$

$$A\tan(\theta_i)^2 + B\tan(\theta_i) + C = 0 \tag{3-7}$$

Among them, A, B, C are functions of 11 connecting rod parameters and azimuth angle $\alpha, \beta, \gamma$

$$\mathrm{A} = \mathrm{w_{i\_x}}(-\mathrm{a_1} + \mathrm{a_3}) + \mathrm{w_{i_y}}(\mathrm{a_4} - \mathrm{a_5}) + \mathrm{w_{i_z}}(\mathrm{a_7}) - \cos(\alpha_{2_i}) \tag{3-8}$$

$$\mathrm{B} = \mathrm{w_{i\_x}}(2\mathrm{a_2}) + \mathrm{w_{i_y}}(2\mathrm{a_6}) + \mathrm{w_{i_z}}(2\mathrm{a_8}) \tag{3-9}$$

$$\mathrm{C} = \mathrm{w_{i\_x}}(\mathrm{a_1} + \mathrm{a_3}) + \mathrm{w_{i_y}}(\mathrm{a_4} + \mathrm{a_5}) + \mathrm{w_{i_z}}(\mathrm{a_7}) - \cos(\alpha_{2\_i}) \tag{3-10}$$

$$\mathrm{X} = \tan(\theta_i/2) \tag{3-11}$$

$$\mathrm{a_1} = -\sin(\alpha_{1\_i})\cos(\delta_i) \tag{3-12}$$

$$\mathrm{a_2} = -\sin(\alpha_{1\_i})\sin(\delta_i)\cos(\gamma_i) \tag{3-13}$$

$$\mathrm{a_3} = -\cos(\alpha_{1\_i})\sin(\delta_i)\sin(\gamma_i) \tag{3-14}$$

$$\mathrm{a_4} = \cos(\alpha_{1\_i})\cos(\delta_i)\sin(\gamma_i) \tag{3-15}$$

$$\mathrm{a_5} = -\sin(\alpha_{1\_i})\sin(\delta_i) \tag{3-16}$$

$$\mathrm{a_6} = \sin(\alpha_{1\_i})\cos(\delta_i)\cos(\gamma_i) \tag{3-17}$$

$$\mathrm{a_7} = -\cos(\alpha_{1\_i})\cos(\gamma_i) \tag{3-18}$$

$$\mathrm{a_8} = \sin(\alpha_{1\_i})\sin(\gamma_i) \tag{3-19}$$

Formula (3-7) is a quadratic equation, including the angle $\theta_i$ of the input main link. From equation (3-7) is a quadratic equation in one variable, we can see that for each branch chain, there are two solutions. Therefore, for each position in the working space of the parallel mechanism, eight possible combination solutions 2×2×2 can be obtained, as shown in Figure 6, but different solutions correspond to different configurations of branch chains. There may be interference between the branches of some solutions, so when the mechanism configuration is uniquely determined, the result of the inverse kinematics solution is also unique.

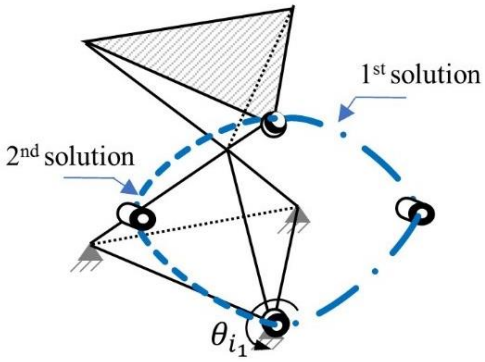


Figure 6 Two possible solutions for each branch

## 3.5 Velocity Jacobian Matrix

In this mechanism, the velocity Jacobian matrix can be obtained by simultaneously deriving the left and right equations

$$\dot{v}_i \cdot w_i + \dot{w}_i \cdot v_i = 0 \tag{3-20}$$

$$\dot{\theta}_i(u_i \times v_i) \cdot w_i + \omega \times w_i \cdot v_i = 0 \tag{3-21}$$

According to the rotation symmetry of the mixed product

$$\omega \times w_i \cdot v_i = \omega \cdot (w_i \times v_i) = -\omega \cdot (v_i \times w_i) \tag{3-22}$$

Relocation

$$\frac{v_i \times w_i}{(u_i \times v_i) \cdot w_i} \omega = \dot{\theta}_i \tag{3-23}$$

Where

$$J_i = \frac{v_i \times w_i}{(u_i \times v_i) \cdot w_i} \tag{3-24}$$

Equation (3-24) obtains the velocity Jacobian matrix of the spherical three-free parallel mechanism.

The motion equation of the mechanism can be written as $\omega = J\dot{\varphi}$, where $\omega$ represents the output angular velocity of the moving platform, $\dot{\varphi}$ represents the input angular velocity, J is the Jacobian matrix, which is the structural parameter $\gamma, \beta, \alpha_{1_1}, \alpha_{1_2}, \alpha_{1_3}, \alpha_{2_1}, \alpha_{2_2}, \alpha_{2_3}, \delta_1, \delta_2, \delta_3$ and the function of the attitude angles $\alpha, \beta, \gamma$ of the moving platform. If the input has a certain deviation $\Delta\omega$, the output of the moving platform will have a corresponding deviation $\Delta\dot{\varphi}$ then $\omega + \Delta\omega = J(\dot{\varphi} + \Delta\dot{\varphi})$, $\Delta\omega = J\Delta\dot{\varphi}$.

According to Euclidean Norm Theory，$\|\Delta\omega\| = \|J\Delta\dot{\varphi}\| \leq \|J\| \cdot \|\Delta\dot{\varphi}\|$和$\|\dot{\varphi}\| = \|J^{-1}\Delta\omega\| \leq \|J^{-1}\| \cdot \|\Delta\omega\|$，therefore

$$\frac{\|\Delta\omega\|}{\|\omega\|} \leq \|J\|\|J^{-1}\| \frac{\|\Delta\dot{\varphi}\|}{\|\dot{\varphi}\|} \tag{3-25}$$

Let $k(J) = \|J\|\|J^{-1}\|$, which is called the condition number of the Jacobian matrix. The condition

number here can be written as

$$k(J) = \|-K_q{}^{-1}J_x\|\|-J_x{}^{-1}K_q\| \tag{3-26}$$

Where

$$\mathrm{J_x} = \begin{bmatrix} (\mathrm{v_1} \times \mathrm{w_1})^{\mathrm{T}} \\ (\mathrm{v_2} \times \mathrm{w_2})^{\mathrm{T}} \\ (\mathrm{v_3} \times \mathrm{w_3})^{\mathrm{T}} \end{bmatrix} \tag{3-27}$$

$$\mathrm{K_q} = \mathrm{diag}(\mathrm{v_1} \times \mathrm{u_1} \cdot \mathrm{w_1} \quad \mathrm{v_2} \times \mathrm{u_2} \cdot \mathrm{w_2} \quad \mathrm{v_3} \times \mathrm{u_3} \cdot \mathrm{w_3}) \tag{3-28}$$

Among them $\| \cdot \|$ represents the Euclidean norm of its matrix parameters, and $\times$ represents the vector product (or cross product). The value of k=1 corresponds to a structure with good dexterity, and the value of k has no upper limit.

### 3.6 Force Jacobian Matrix

Assuming that the virtual displacement of the drive motor is $\delta q_i$, the virtual displacement of the end of the moving platform is $\delta X$, the torque of each drive joint is $\tau_i$, and the torque of the end of the moving platform is F. According to the principle of virtual displacement [7], the work of each joint is equal to the work of the end effector, then

$$\tau^T \delta q = F^T \delta X \tag{3-29}$$

Substitute the geometric constraint relation of the virtual displacement $\delta q_i$ and $\delta X$

$$\delta X = J dq \tag{3-30}$$

Therefore

$$\tau = J^T F \tag{3-31}$$

Let $G = (J^{-1})^T$, called force Jacobian matrix, which represents the relationship between the external torque at the end of the moving platform and the driving input torque.

It can be seen that the transpose of the inverse of the velocity Jacobian matrix is the force Jacobian matrix. If the input torque has a small change $\Delta\omega$, the external torque received by the moving platform will correspondingly have a small change $\Delta\dot{\varphi}$. In the same way, the condition number of the force Jacobi matrix can be obtained by deriving the condition number of the velocity Jacobian matrix.

$$\frac{\|\Delta F\|}{\|F\|} \leq k(G)\frac{\|\Delta\tau\|}{\|\dot{\tau}\|} \tag{3-32}$$

Among them, $k(G) = \|G\|\|G^{-1}\|$, which is called the condition number of the force jacobi matrix. The condition number of the force jacobi matrix can measure the transmission accuracy between the input torque and the output torque. The value range of $k(G)$ is $[1, +\infty]$. The smaller the value, the higher the transmission accuracy. The condition number here can be written as

$$k(G) = -{K_q}^{-1}J_x \tag{3-33}$$

where

$$J_x = \begin{bmatrix} (v_1 \times w_1)^T \\ (v_2 \times w_2)^T \\ (v_3 \times w_3)^T \end{bmatrix} \tag{3-34}$$

$$K_q = \mathrm{diag}(v_1 \times u_1 \cdot w_1 \quad v_2 \times u_2 \cdot w_2 \quad v_3 \times u_3 \cdot w_3) \tag{3-35}$$

# 4. Main methods

## 4.1 Genetic algorithm and multi-objective optimization

Multi-objective optimization is a common problem in all fields of reality. It is not possible to optimize each object at the same time, and each object must have its own weight. The weight distribution problem needs to be determined based on known information. The genetic algorithm designed and proposed according to the evolutionary law of organisms in nature can maintain the globality of the solution through operations such as mutation, so as to avoid obtaining a locally optimized solution. Therefore, the idea of genetic algorithm is used to perform multi-objective optimization of three-degree-of-freedom spherical parallel mechanism [8].

In the parameter optimization process, three objective functions are considered. The first goal is that the working space is as close as possible to the range of motion of the human shoulder joint; the second goal is to have as much dexterity as possible everywhere in the working space; the third goal is to minimize the torque of the three input shafts. The torque is beneficial to reduce the power demand of the drive motor, thereby reducing the overall weight and size of the shoulder joint [9]. Using genetic algorithm, the structural parameter design of the parallel spherical mechanism is carried out while satisfying the three goals as much as possible.

Genetic algorithms (GA) are heuristic methods that consist in optimization procedures as inspired in natural evolution [10]. In GA, an initial random population needs to be created. The characteristics of each solution are used in equivalent chromosomes. Each solution is evaluated and classified according to how well it satisfies the objective function and then it is assigned a probability of reproduction. The fittest individuals are more likely to be reproduced (selection), and thus they inherit those characteristics. The combination (crossover) of the parent genes yields to a consecutive generation (replacement). Mutation can occur in the chromosomes of some individuals. It is projected that some individuals of this new generation will have inherited the best characteristics of their parents and will be a better solution to the problem. This new population goes through the same process and this cycle is repeated until all the members share the same genetic information. This last generation is the best solution to the optimization problem [11]. A

genetic algorithm is stopped when the population converges to an optimal solution or when a maximum number of generations is reached, Figure 7 .

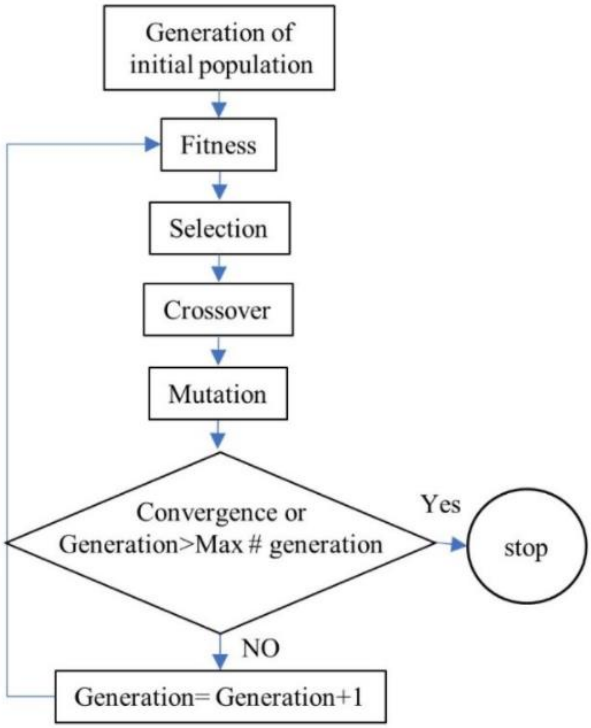


Figure 7 A flow chart of a genetic algorithm optimization.

Genetic algorithms require objective and fitness functions. The objective function defines the optimal condition and the fitness function assesses how well a specific solution satisfies the objective function and assigns a real value to that solution [12].

Formerly, the information of the individuals was encoded in bit strings called Binary-coded, but nowadays the individuals are coded using real numbers. Real-coded GA usually achieves better results than Binary-coded GA [13].

The selection process consists in taking two parents to create offspring. The objective is to provide to the fitter individuals a greater chance of reproduction expecting that their offspring will have higher fitness. Typical types of selection scheme are the proportionate selection and the ordinal-based selection. In the proportionate based selection, the individuals are picked up based on their fitness values that are relative to the fitness of the other individuals. The ordinal-based selection selects individuals by considering their rank within the population.

The crossover combines two different individuals to generate new offspring [14]. Many crossover methods exist, and the most common is single-point crossover. In this work, a linear crossover is used. Two parents are selected as p1 and p 2 and three offsprings are generated as 0.5 p1 + 0.5p2, 1.5 p 1 - 0.5p2, -0.5 p1 +1.5p2 respectively. Then, the three offspring are evaluated and the best two are selected for the next generation.

Mutation consists in a random modification of a gene during reproduction. In general, the mutation prevents convergence to a local optimum [15]. The mutation operator is applied with a small probability. In this work, a non-uniform mutation is used.

Multi-objective optimization commonly involves multiple conflicting objectives that must be considered simultaneously and there is a set of mathematically equally good solutions. These set of solutions are known as nondominated or Pareto optimal set. The set of solutions forms the Pareto optimal front. The characteristic of a Pareto optimal solution is that any change in the values of the solution will not improve any of the objective functions.

The concept of dominance or domination is used in most of the optimization algorithms. If there are *N* objective functions, a solution x(1) dominates another solution x(2) if the two following conditions are true [16]:

1. The solution x(1) is no worse than x(2) in all objectives.

2. The solution x(1) is better than x(2) in at least one objective.

A solution x(1) is Pareto-optimal if is nondominated with respect to the search space (or feasible region) [17].

Many evolutionary algorithms have been proposed over the years to solve multi-objective optimization problems. In this work, it is used a controlled elitist non-dominated sorting GA (CENSGA). The algorithm of CENSGA is based in NSGA-II, but there is a difference in the selection approach that improves the convergence to the Pareto front.

The CENSGA algorithm works as follows. First, a random Pt population of size N is formed. From this population, Q offsprings are created using the common GA operators (crossover, mutation). Then, a combined Rt population (Pt ∪ Qt) of size 2N is formed. The population Rt is sorted according to non-

domination and different non-dominated fronts are created. The first non-dominated front is formed only by elements non-dominated with respect to Rt. The second non-dominated front is formed by elements dominated by just one solution. All the elements of Rt are assigned a front in a similar fashion [18]. The crowding distance is calculated for every element of Rt. Then N elements are selected from Rt to form the next generation Pt+1. The maximum number of elements selected from i-th non-dominated front is defined by a geometric distribution

$$n_i = N\frac{1-r}{1-r^K}r^{i-1}$$

where r is the reduction ratio (r<1) and K is the number of non-dominated fronts.

ni denotes the maximum allowable number of individuals taken from the i-th front. If ni is larger than the number of elements in the i-th front, then all the elements of this front are chosen and the remaining slots are added to ni+1. But if ni is smaller than the number of elements in the front, ni the elements are chosen using a crowded binary tournament selection. The crowded binary tournament takes two elements and returns the one with the bigger crowding distance. GA operators are applied to the new population of Pt+1 to form Qt+1 and are combined to form Rt+1 and the described process is repeated for a specific number of generations. The result of this process is the Pareto front, this means a set of optimal solutions. CENSGA algorithm is summarized in Figure 8.

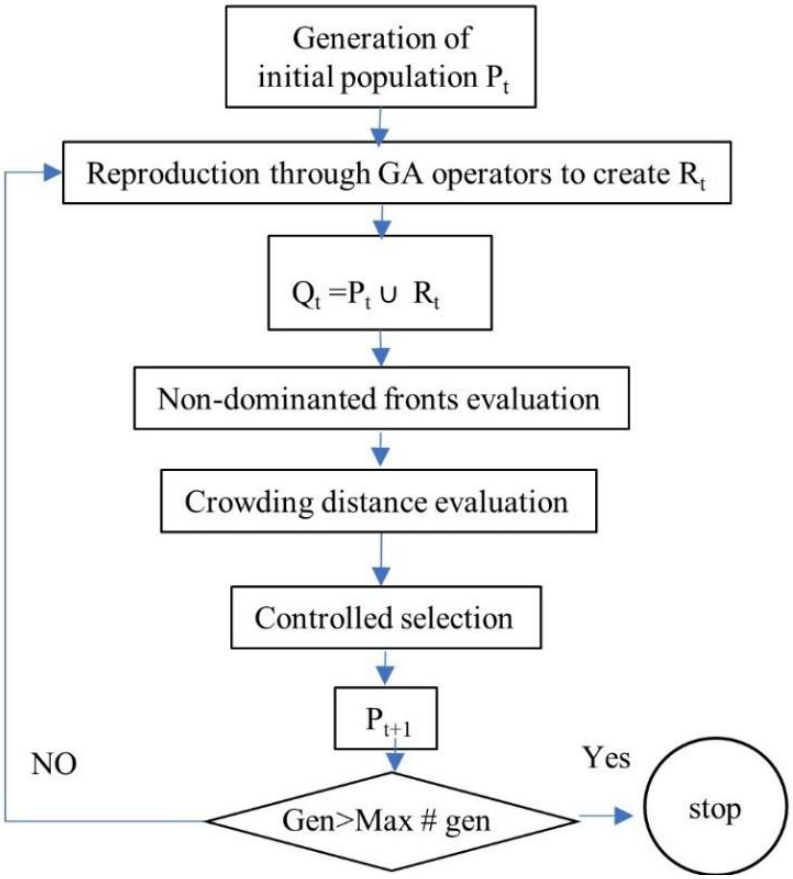


Figure 8 A flow diagram of the CENSGA algorithm.

## 4.2 Optimization objective function

The optimization design steps of the structural parameters of the spherical parallel mechanism based on the genetic algorithm are as follows: There are three optimization objectives for the spherical parallel mechanism with three degrees of freedom, working space, dexterity, and maximum torque, which are multi-variable and multi-objective optimization. The 11 structural parameters that need to be optimized for this spherical parallel bionic shoulder joint mechanism are defined as follows:

$$\gamma, \beta, \alpha_{1\_1}, \alpha_{1\_2}, \alpha_{1\_3}, \alpha_{2\_1}, \alpha_{2\_2}, \alpha_{2\_3}, \delta_1, \delta_2, \delta_3$$

The first goal of optimization is to maximize the working space. First, discretize the range of motion of the human shoulder joint at every 10°, as shown in Figure 2-3, a total of 12x11x10=1320 points, and then judge each discretized point Whether the equation (3-7) has a solution, then count the number of points that have a solution to the one-variable quadratic equation and record it as g_1, select the appropriate structure parameter value to make g_1 the largest, for simplicity, multiply g_1 by -1 and it minimize. Take flexion and extension exercise as an example, the required range of motion is 110° of arc, discrete in 10° segments. The objective function of the workspace can be defined as:

$$g_1 = \sum h(Q), h = \begin{cases} 1 & \text{if } \tan(\theta_i) \text{ in Eq. } (3-7) \text{ is real} \\ 0 & \text{if } \tan(\theta_i) \text{ in Eq. } (3-7) \text{ is not real} \end{cases} \quad (4\text{-}1)$$

Where $g_1$ is discretized from the above, the maximum value of this function is 12.

The second goal of optimization is related to the movement accuracy of the parallel mechanism. Motion accuracy is related to the condition number of the Jacobian matrix (also related to dexterity). The dexterity is defined as:

$$k = \left\| -K_q{}^{-1} J_x \right\| \left\| -J_x{}^{-1} K_q \right\| \quad 1 \le k \le \infty \quad (4\text{-}2)$$

where

$$J_x = \begin{bmatrix} (v_1 \times w_1)^T \\ (v_2 \times w_2)^T \\ (v_3 \times w_3)^T \end{bmatrix} \quad (4\text{-}3)$$

$$K_q = \mathrm{diag}(v_1 \times u_1 \cdot w_1 \quad v_2 \times u_2 \cdot w_2 \quad v_3 \times u_3 \cdot w_3) \tag{4-4}$$

Among them $\| \bullet \|$ represents the Euclidean norm of its matrix parameters, and $\times$ represents the vector product (or cross product).

The range of motion of the human shoulder joint is discretized every 10°, as shown in Figure 2-3, a total of 12x11x10=1320 points, and then for each discretized point, the value of the velocity Jacobian condition number k is calculated, and the value of k is in [1,10] The ratio in the interval is used as the dexterity evaluation index $g_2$.

The objective function of dexterity can be defined as:

$$g_2 = -\frac{\sum_{i=1}^{n} x_i k_i}{n} \quad x_i = \begin{cases} 1 & k_i \in [1,10] \\ 0 & k_i \in (10, +\infty] \end{cases} \tag{4-5}$$

The third optimization goal is related to the torque required to perform the flexion and extension movement. Due to the low acceleration required during movement and the low mass of the prosthetic device, the inertial effect can be ignored, and static analysis can be performed on each position in the defined trajectory with limited computational cost. First, the range of motion of the human shoulder joint is discretized every 10°, as shown in Figure 2-3, a total of 12x11x10=1320 points, and then the value of $\tau$ is calculated for each discretized point, and appropriate structural parameter values are selected to make $g_3 = \max(\tau)$ is the smallest, the objective function can be defined as:

$$g_3 = \max(\tau) \tag{4-6}$$

$$\tau = J^T F \tag{4-7}$$

Where J is the velocity Jacobian matrix and the expression is

$$J = -{K_q}^{-1} J_x \tag{4-8}$$

F is the torque generated by the weight of the prosthetic device (15N), the hand (5N) and the load (5N) that it bears in consideration of its corresponding lever arm.

### 4.3 Optimization constraints

Since the inverse kinematics solution of the parallel mechanism has eight different solutions (each branch has two different solutions), it is necessary to establish an equation to limit the branches of the same solution during the entire optimization process. In addition, it can be seen from Figure 3-2 that in order to switch from one branch to another, it is only possible to align the connecting rods of the branch chain. At this time, the mechanism is in a strange position, at this time $(\overrightarrow{w_i} \times \overrightarrow{u_i}) \cdot \overrightarrow{v_i} = 0$, so to avoid singularity, the constraint is defined as sign $sign\left((\overrightarrow{w_i} \times \overrightarrow{u_i}) \cdot \overrightarrow{v_i}\right)$ to remain constant.

Second, in order to ensure that the positions of the motors do not overlap, the limit between $\delta_i$ is set to a minimum angle of 100 degrees between the fixed points so that the motors can be installed.

$$h_1 = |\delta_1 - \delta_2| \geq 100° \quad (4\text{-}9)$$

$$h_2 = |\delta_2 - \delta_3| \geq 100° \quad (4\text{-}10)$$

$$h_3 = |\delta_1 - \delta_3| \geq 100° \quad (4\text{-}11)$$

### 4.4 Optimization definition

The total design parameters are $\gamma, \beta, \alpha_{1\_1}, \alpha_{1\_2}, \alpha_{1\_3}, \alpha_{2\_1}, \alpha_{2\_2}, \alpha_{2\_3}, \delta_1, \delta_2, \delta_3$, the total optimization problem definition is

$$\min \quad g_1, g_2, g_3$$

$$\text{subject to } h_1 \geq 100, h_2 \geq 100, h_3 \geq 100, \quad sign\left((\overrightarrow{w_i} \times \overrightarrow{u_i}) \cdot \overrightarrow{v_i}\right) = const$$

### 4.5 Solution settings

Using the MATLAB NSGA-II toolbox, set a random population of 100 individuals and a reduction rate of 0.5. The maximum number of iterations is 200. Using linear crossover and non-uniform mutation genetic operators, the mutation probability is 0.5%.

# 5. Numerical results

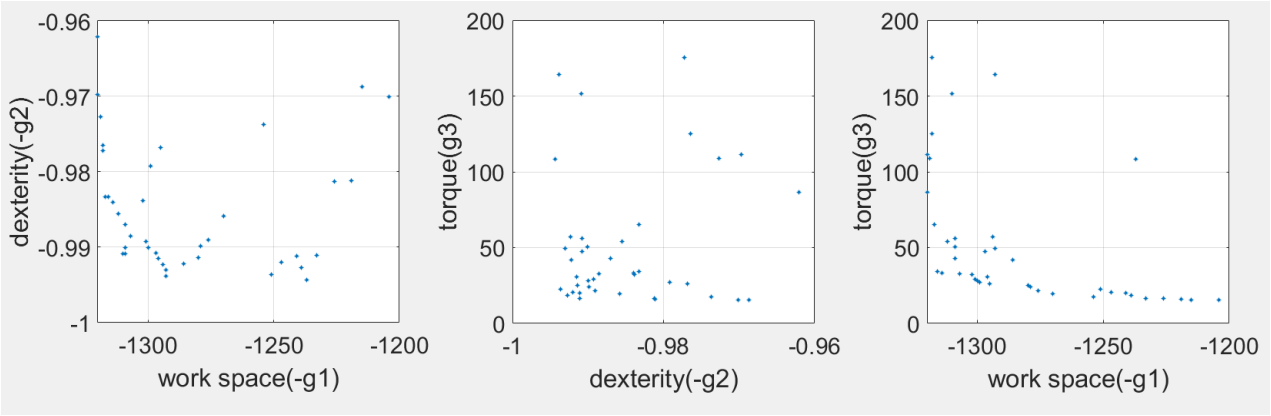


Figure 9 Optimization result graph

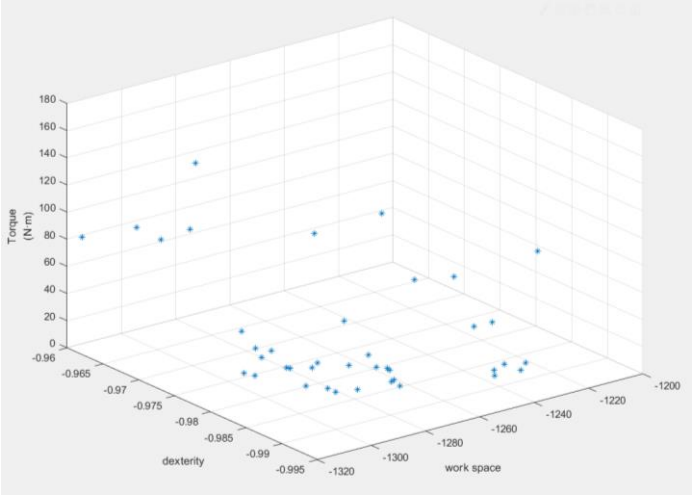


Figure 10 Optimization result graph in 3D

# 6. Discussions

The optimization results are shown in Figure 9 and Figure 10. Each blue dot represents three optimization target values corresponding to a set of parameter results. Figure 9(a) shows the relationship between the working space and dexterity of each group of parameters. The largest working space corresponds to the abscissa value of -1320, and the ordinate value corresponding to the highest dexterity is -1. The shoulder joint dexterity is required to be high and the working space is large, so in Figure 9(a), take the point with the largest dexterity and working space, which is the lower left point; as shown in Figure 9(b) It is the relationship between dexterity and maximum joint torque. The abscissa value corresponding to the

highest dexterity is -1, and the ordinate value corresponding to the maximum joint torque is 100. We require the shoulder joint dexterity to be high and the maximum joint torque to be small. Therefore, in Figure 9(b), the point with the greatest dexterity but the smallest joint torque is also the lower left point; Figure 9(c) shows the relationship between the working space and the maximum joint torque. The maximum corresponding abscissa value of the working space is -1320, and the ordinate value corresponding to the maximum joint torque is 100. We require a large shoulder joint working space and a small maximum joint torque, so take the work in Figure 9(c) The point with the largest space but the smallest joint torque is also the lower left point; Figure 10 shows the relationship between working space, dexterity and maximum joint torque, expressed by x-y-z three-axis coordinates , The x-axis coordinate value corresponding to the largest working space is -1320, the y-axis coordinate value corresponding to the highest dexterity is -1, and the z-axis coordinate value corresponding to the maximum joint torque is 100. We require a large shoulder joint working space and dexterity It should be high and the maximum joint torque should be small, so in Figure 9(d), take the point with the largest workspace, the highest dexterity, and the smallest joint torque, which is also the lower left point.

There are also three possible distributions at the lowest corner point: the working space is large and the dexterity is high, but the maximum joint torque is not the smallest; the working space is large, the maximum joint torque is small, but the dexterity is not the highest; the dexterity is very high, the maximum joint torque is small, but the working space is not the maximum. Generally speaking, the point that satisfies the working space is selected first, followed by high dexterity, and finally the maximum joint torque is considered.

After comparing the solutions, a set of parameters with the objective function value $g_1$=-1320, $g_2$=-0.99 and $g_3$=4.5(N·m) is selected. Table 2 shows the 11 parameter values associated with this solution.

Table 2 parameter values

| $\gamma$ | $\beta$ | $\alpha_{1\_1}$ | $\alpha_{1\_2}$ | $\alpha_{1\_3}$ | $\alpha_{2\_1}$ |
|---|---|---|---|---|---|
| 73.97034 | 74.02084 | 65.55052 | 89.83113 | 81.71658 | 66.60625 |
| $\alpha_{2\_2}$ | $\alpha_{2\_3}$ | $\delta$1 | $\delta$2 | $\delta$3 | |
| 83.08663 | 81.55116 | 68.03214 | 186.1973 | 295.7946 | |

# 7. Reference

[1]国务院关于印发“十三五”加快残疾人小康进程规划纲要的通知. 000014349/2016-00167

[2]Leal-Naranjo J A, Ceccarelli M, Torres-San-Miguel C R, et al. Multi-objective optimization of a parallel manipulator for the design of a prosthetic arm using genetic algorithms[J]. Latin American Journal of Solids and Structures, 2018, 15(3).

[3]Merlet J P. Parallel robots[M]. Springer Netherlands, 2014.

[4]黄真,赵永生,赵铁石.高等空间机构学[M].北京:高等教育出版社,2014.

[5]赵铁军，赵明扬，单光坤,等.仿人机器人柔性腰部机构研究[J]. 机器人, 2003, 25(2): 101-104.

[6]Ceccarelli M. Fundamentals of the mechanics of robots[M]//Fundamentals of Mechanics of Robotic Manipulation. Springer, Dordrecht, 2004: 73-240.

[7]熊有伦，丁汉，刘恩沧.机器人学.北京：机械工业出版社.1993：36-40 88.91 110-1 1 3

[8]Leal-Naranjo J A, Ceccarelli M, Torres-San-Miguel C R, et al. Multi-objective optimization of a parallel manipulator for the design of a prosthetic arm using genetic algorithms[J]. Latin American Journal of Solids and Structures, 2018, 15(3).

[9]Leal-Naranjo J A, Ceccarelli M, Torres-San Miguel C R. Mechanical design of a prosthetic human arm and its dynamic simulation[C]//International Conference on Robotics in Alpe-Adria Danube Region. Springer, Cham, 2016: 482-490.

[10] K.P. Chong and S. Zak, An Introduction to Optimization, 4th Edition, Wiley.

[11] Fogel, D. (1994). An introduction to simulated evolutionary optimization, IEEE Transactions on neural networks 5(1): 3-14.

[12] Coello, C. A. C., Lamont, G. B. and Veldhuizen, D. A. V. (2007). Evolutionary algorithms for solving multi-objective problems, Springer.

[13] Deb, K. and Kumar, A. (1995). Real-coded genetic algorithms with simulated binary crossover: studies on multimodal and multiobjective problems, Complex systems 9: 431-454.

[14] Blum, C., Chiong, R., Clerc, M., Jong, K. D., Michalewicz, Z., Neri, F. and Weise, T. (2012). Evolutionary optimization. Variants of Evolutionary Algorithms for Real-World Applications, Springer

Berlin Heidelberg: 1-29.

[15] Cabrera, J. A., Simon, A. and Prado, M. (2002). Optimal synthesis of mechanisms with genetic algorithms, Mechanism and machine theory 37: 1165-1177.

[16] Deb, K. (2014). Multi-objective optimization. Search methodologies, Springer US: 403-449.

[17] Coello, C. A. C. (2015). Multi-objective evolutionary algorithms in real-world applications: Some recent results and current chalenges. Advances in Evolutionary and Deterministic Methods for Design, Optimization and Control in Engineering and Sciences, Springer International Publishing: 3-18.

[18] Elarbi, M., Bechikh, S., Said, L. B. and Datta, R. (2017). Multi-objective optimization: Classical and evolutionary approaches. Recent advances in evolutionary multi-objective optimization. Springer International Publishing: 1-30.